A non-differential elastomer curvature sensor for softer-than-skin electronics

2011 Smart Mater. Struct. 20 105017

(http://iopscience.iop.org/0964-1726/20/10/105017)

Smart Mater. Struct. **20** (2011) 105017 (7pp) doi:10.1088/0964-1726/20/10/105017

A non-differential elastomer curvature sensor for softer-than-skin electronics

C Majidi[1,3], **R Kramer**[1,2] **and R J Wood**[1,2]

[1] School of Engineering and Applied Sciences, Harvard University, Cambridge, MA 02138, USA
[2] Wyss Institute for Biologically Inspired Engineering, Harvard University, Boston, MA 02115, USA

E-mail: cmajidi@andrew.cmu.edu

Received 22 February 2011, in final form 13 July 2011
Published 31 August 2011
Online at stacks.iop.org/SMS/20/105017

Abstract
We extend soft lithography microfabrication and design methods to introduce curvature sensors that are elastically soft (modulus 0.1–1 MPa) and stretchable (100–1000% strain). In contrast to existing curvature sensors that measure differential strain, sensors in this new class measure curvature directly and allow for arbitrary gauge factor and film thickness. Moreover, each sensor is composed entirely of a soft elastomer (PDMS (polydimethylsiloxane) or Ecoflex®) and conductive liquid (eutectic gallium indium, eGaIn) and thus remains functional even when stretched to several times its natural length. The electrical resistance in the embedded eGaIn microchannel is measured as a function of the bending curvature for a variety of sensor designs. In all cases, the experimental measurements are in reasonable agreement with closed-form algebraic approximations derived from elastic plate theory and Ohm's law.

(Some figures in this article are in colour only in the electronic version)

1. Introduction

Elastomer-based sensors, microelectronics, and artificial skin represent the next stage in a technological progression from rigid microelectronics to MEMS to soft microfluidics. This new class of active films will be soft (modulus $\sim$ 0.01–1 MPa), durable, impact resistant and remain electronically functional when stretched to several times their natural length. Applications that are currently being explored include joint angle monitoring in soft active orthotics (Park *et al* 2011), a stretchable keyboard interface for wearable computing (Kramer *et al* 2011), contact detection in soft autonomous robots (Seok *et al* 2010), and curvature sensing for folding programmable matter (Hawkes *et al* 2010).

In contrast to existing thin-film solutions that are flexible but not stretchable[4], this next generation of sensors and circuits must be able to conform to dramatic but reversible changes in shape and changes in rigidity without interfering with the natural mechanics of the host. One now well-established method is to pre-buckle circuit elements and wiring into wavy patterns that unfold as the supporting elastic substrate is being stretched (Rogers and Huang 2009, Khang *et al* 2006, Kim *et al* 2008). Though typically limited to 50–100% strains, this versatile approach allows stretchable functionality with a broad range of thin-film metals, semiconductors, and polymers. For hyperelastic strains of 100–1000%, electronic functionality is achieved by embedding microchannels of conductive liquid in a thin elastomer film (Dickey *et al* 2008). This latter approach builds on the manufacturing techniques (Xia *et al* 1999) developed for elastomer-based microfluidics (Quake and Scherer 2000) and has been utilized for strain sensing (Kim *et al* 2008, Cheng and Wu 2011), pressure sensing (Park *et al* 2010), and a mechanically tunable antenna (So *et al* 2009, Cheng and Wu 2010).

We extend the principle of liquid embedded elastomers to introduce a stretchable thin-film curvature sensor (figure 1). As illustrated in figure 2(a), the sensor is composed of two coplanar elastic films that are connected along their edges and at their center by a strut. One of the films contains a microchannel of conductive liquid (Dickey *et al* 2008) (eutectic gallium indium, eGaIn) that is oriented along the

[3] Present address: Department of Mechanical Engineering, Carnegie Mellon University, Pittsburgh, PA 15213, USA.
[4] Manufacturers include Images Scientific Instruments (Bi-Flex SensorsTM), Flexpoint Sensor Systems (Bend Sensor®), and Tekscan, Inc. (FlexiForce® Sensors).

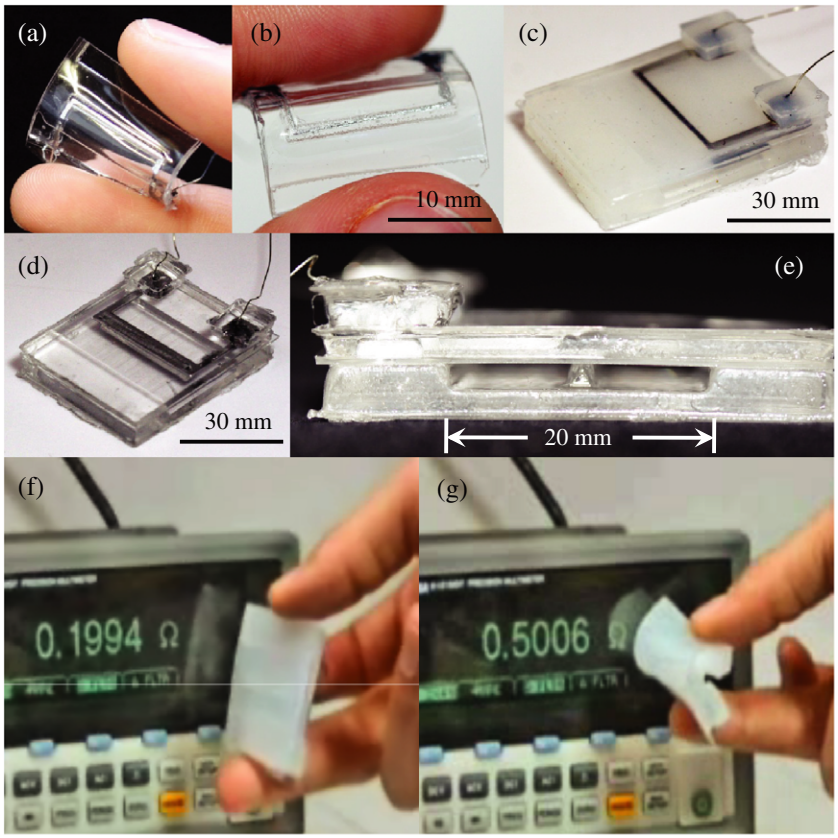

Figure 1. Bending a micropatterned elastomer changes the electrical resistance of an embedded conductive liquid microchannel; experiments are performed on a ((a), (b)) 1.3 mm thick PDMS sensor, a 6 mm thick (c) Ecoflex®, and ((d), (e)) PDMS sensors; ((f), (g)) bending the Ecoflex® sensor.

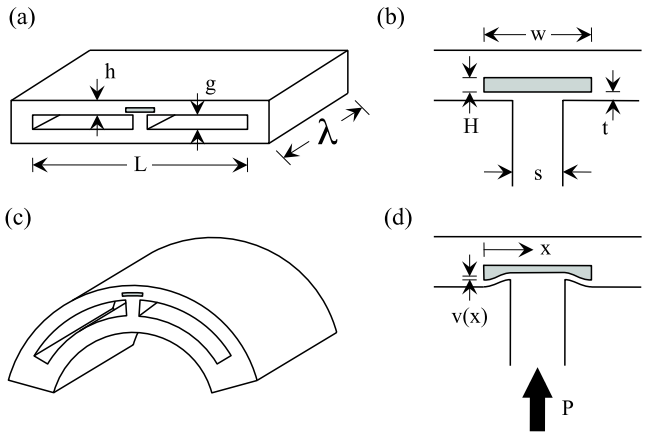

Figure 2. (a) The curvature sensor is composed of two thin films with thickness h, length L, and width d that are separated by a gap g and bonded along their two ends as well as along their midline by a strut of width s. (b) One of the films contains a microchannel of height H and width w located a distance t above the strut. (c) Bending induces a compressive force P that (d) causes the embedded channel to collapse.

strut. Bending the sensor induces a compressive force in the strut, which consequently exerts a pressure on the embedded channel. This pressure causes the cross-section of the channel to elastically deform and, following Ohm's law, leads to a change in electrical resistance.

2. Theory

Referring to figure 2(a), two elastomer films of thickness h are separated by a gap of height g and length L. As shown in figure 2(b), the top film contains an embedded channel with a width w, height H, length λ, and a bottom wall thickness t. The two plates are connected along both their edges as well as along a strut of width s, height g, and a length λ that is co-linear with the embedded channel.

Bending the sensor with a small or moderate curvature κ (see figure 2(c)) causes the outer film to stretch with a membrane strain $\varepsilon_0 = \kappa(g+h)/2$ and the inner film to shorten with an equal and opposite membrane strain $-\varepsilon_0$.[5] According to Hooke's law (Gere and Timoshenko 1984), bending will induce an internal force of magnitude $f = B\lambda h(g+h)\kappa/2$, where B is the bending modulus[6] and it is assumed that the plates have the same length λ as the strut and channel.

A free body diagram of the plates and strut is presented in figure 3. The axial force f induces a compressive force $P = 2f\sin(\kappa L/2)$ in the strut. If the channel is wider than

[5] As in classical plate theory, pure bending indicates the absence of net stretching through the entire cross-section of the sensor and membrane strain denotes the average axial strain normal along each individual film cross-section.

[6] For a thin plate, stress is restricted to the plane of the plate and strain is restricted to the plane of bending. Hence, the bending modulus B is defined as the tensile (Young's) modulus E divided by $1-\nu^2$, where ν is Poisson's ratio, i.e. $B = E/(1-\nu^2)$.

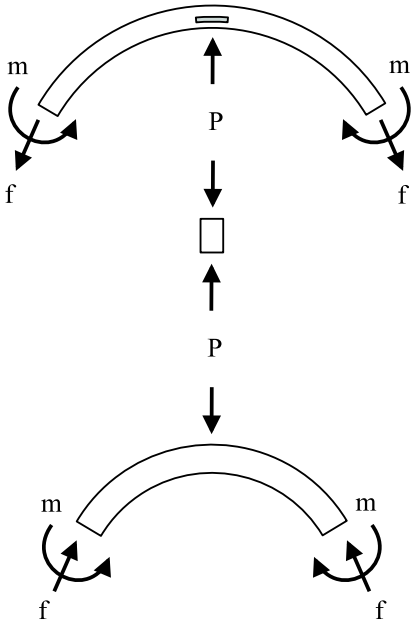

Figure 3. Free body diagram of plates and strut.

the strut ($s < w$) then this bending-induced compression will cause the strut to pierce into the channel as illustrated in see figure 2(d). Alternatively, if the strut is wider ($s > w$), then the elastomer will deform around the channel. In either case, the force P will reduce the cross-sectional area A of the embedded channel and cause the electrical resistance R to decrease by an amount ΔR.

In summary, mechanical coupling between plate bending and internal pressure allows the magnitude $|\kappa|$ to be estimated from the corresponding change ΔR within the embedded channel. The sensor output ΔR is proportional to the electrical resistivity ρ of the conductive liquid. eGaIn has a resistivity of $\rho = 29.4 \times 10^{-8}\ \Omega\ \mathrm{m}^{-1}$ (Dickey *et al* 2008) that is comparable to other metal alloys and several orders of magnitude lower than the resistivity of conductive inks and carbon-based liquids.

2.1. Pressure mode ($s > w$)

When the strut is wider than the channel, pressure from the strut will be distributed around the channel and compress the surrounding elastomer. This loading condition is similar to that previously addressed in (Kramer *et al* 2011, Park *et al* 2010), in which pressure p is exerted on the surface of an elastomer half-space embedded with a microchannel of conductive liquid. According to that analysis, the relative change in electric resistance is approximately

$$\frac{\Delta R}{R_0} = \left\{1 - \frac{2wp}{BH}\right\}^{-1} - 1, \tag{1}$$

where $R_0 = \rho\lambda/wH$ is the original (undeformed) electrical resistance and ρ is the electrical resistivity of the liquid.

The pressure p is estimated by simply dividing the strut force P by its cross-sectional area: $p = P/s\lambda$. Substituting in the values for P, f, and p into ΔR,

$$\Delta R = \frac{\rho\lambda}{wH}\left\{\frac{1}{1 - \alpha\kappa h \sin(\kappa L/2)} - 1\right\}, \tag{2}$$

where

$$\alpha = \frac{2w(g+h)}{Hs}. \tag{3}$$

The constants w and H correspond to the original dimensions of the embedded channel, prior to bending, and are thus independent of the curvature. The approximation (2) is only valid when $\alpha\kappa h \sin(\kappa L/2) < 1$, which follows from the constraint $2wp/BH < 1$ (Park *et al* 2010). Physically, this bound arises from the unilateral constraint that prevents the collapsing channel walls from interpenetrating.

As expected, the electrical resistance increases monotonically with increasing absolute curvature $|\kappa|$ and increases by the same amount regardless of whether κ is positive or negative. Moreover, the solution suggests that ΔR increases with increasing film thickness h, gap height g, and gap length L and decreasing strut width s. Interestingly, ΔR is invariant to B, although the bending modulus will control how much moment is required to reach a prescribed curvature κ.

For low or moderate bending curvatures, we simplify (2) by invoking the small angle approximation $\sin(\kappa L/2) \approx \kappa L/2$ and noting that $\alpha\kappa^2 hL/2 \gg 1$. According to the Taylor expansion $1/(1-\chi) \approx 1 + \chi + \mathcal{O}(\chi^2)$, it follows that $\Delta R/R_0 \approx \alpha\kappa^2 hL/2$:

$$\frac{\Delta R}{R_0} \approx \left(\frac{\kappa}{\kappa_1}\right)^2, \tag{4}$$

where

$$\kappa_1 = \sqrt{\frac{Hs}{whL(g+h)}}. \tag{5}$$

The characteristic curvature κ_1 corresponds to the sensitivity of the sensor. For example, the electrical resistance increases by one per cent when κ changes by an amount $0.1\kappa_1$.

2.2. Collapse mode ($s < w$)

When $s < w$, the strut is modeled as a rigid link supported by two flexible plates of thickness t, width λ, and length $\xi = (w-s)/2$. Compression in the strut will cause the plates to deflect into the channel by an amount

$$v(x) = \frac{Px^2\{3(w-s)/4\lambda - x\}}{B\lambda t^3}, \tag{6}$$

where x is the distance from the channel sidewall (see figure 1(d)). This estimate is derived using the equations for beam theory presented in (Gere and Timoshenko 1984). Evaluating $v(x)$ at $x = \xi$ indicates the distance v_0 that the strut pierces into the channel:

$$v_0 = \frac{P(w-s)^3}{16B\lambda t^3}. \tag{7}$$

The total change in channel cross-section can be estimated as

$$\Delta A = v_0 s + 2\int_0^{\xi} v(x)\,\mathrm{d}x = \frac{P(3s+w)(w-s)^3}{64B\lambda t^3}. \tag{8}$$

This results in an electrical resistance

$$R = \rho\lambda/(wH - \Delta A). \tag{9}$$

Substituting in the values for ΔA, P, and f yields an estimate of the total change in electrical resistance:

$$\Delta R = \frac{\rho\lambda}{wH}\left\{\frac{1}{1-\beta\kappa h\sin(\kappa L/2)} - 1\right\}, \tag{10}$$

where

$$\beta = \frac{(g+h)(3s+w)(w-s)^3}{64wHt^3}. \tag{11}$$

As in (2), ΔR monotonically increases with increasing curvature $|\kappa|$, plate thickness h, gap height g, and gap length L. However, it is no longer monotonically dependent on strut width s.

When κ is small or moderate, $\Delta R/R_0$ reduces to the quadratic form

$$\frac{\Delta R}{R_0} \approx \left(\frac{\kappa}{\kappa_2}\right)^2, \tag{12}$$

where

$$\kappa_2 = \sqrt{\frac{32whLHt^3}{(g+h)(3s+w)(w-s)^3}}. \tag{13}$$

As in the previous case, the characteristic curvature κ_2 corresponds to the sensitivity of the sensor. The sensor geometries w, h, L, H, t, g, and s must be selected so that κ_2 is near the lower bound of anticipated bending curvatures.

2.3. Non-linear plate deflection

For large bending curvatures, the compressive membrane force f induced within the inner film will exceed its critical buckling strength f_{cr} and the film will buckle. For a thin plate clamped at both ends, first-mode buckling corresponds to a critical strength $f_{cr} = 4\pi^2 Bwh^3/3L^2$ (Gere and Timoshenko 1984). Plate buckling limits the compressive force in the strut to a value $P_{cr} = 2f_{cr}\sin(\kappa L/2)$. In general, $P = \min(2f\sin(\kappa L/2), P_{cr})$, which leads to a deviation from equations (2) and (10) when $|\kappa|$ exceeds the critical value $\kappa_{cr} = 2f_{cr}/B\lambda h(g+h)$. Substituting this value of P into the expressions for strut p and ΔA leads to new algebraic formulas for ΔR in the buckling regime where $|\kappa| > \kappa_{cr}$.

It is important to note that in addition to the axial load f, the plates are subject to an internal bending moment. This combined loading leads to non-linear deflection even when $f < f_{cr}$ (see figure 4). This 'premature' subcritical plate buckling can cause the gap to collapse and redirects compressive stress away from the strut and toward the new plate contacts. Hence, P_{cr} and κ_{cr} represent upper bounds and the corresponding theoretical predictions for ΔR may overestimate the true change in electrical resistance.

3. Experiment

Curvature measurements are performed on three elastomer sensors, two that are 6 mm thick and a third that is 1.3 mm thick. The 6 mm thick samples are produced by pouring uncured PDMS (Dow Corning) or soft silicone rubber (EcoFlex® 0030, SmoothOn) into a 3D printed mold (Connex 500, Objet Ltd). The 1.3 mm samples are produced by spin coating uncured PDMS on glass slides that are covered with laser-cut (VersaLaser system, Universal Laser Systems) adhesive films. After curing, the rubber sheets are released and bonded together either with oxygen plasma treatment (for PDMS, Plasma Prep IIITM, SPI Supplies) or a thin layer of uncured rubber (for EcoFlex®). Next, a syringe is used to fill the embedded channels with eutectic Gallium Indium (eGaIn, 99.9% pure, Sigma-Aldrich). Wire is inserted into the ends of the channels, which are then sealed with a drop of uncured rubber.

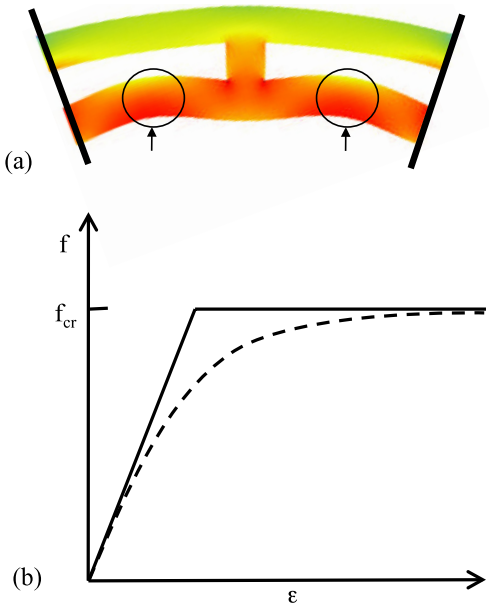

Figure 4. The inner plate is loaded under combined axial stress and moment, which (a) leads to non-linear deflection from the perfect circular arc even when the axial load is below the critical value f_{cr}. An (exaggerated) qualitative representation of the axial load f as a function of axial strain ε depicting both ideal buckling and non-linear deviation induced by combined moment loading.

The change in electrical resistance ΔR is measured as a function of bending curvature κ. Rigid plastic clamps are fitted around the bonded edges of the elastomer. Pure bending is induced by positioning the base of the plastic clamps at various geometrically defined orientations. These positions and orientations are carefully selected so that the sensor bends into a circular arc of radius $r = 1/\kappa$ without stretching. The clamps are sequentially oriented from 0° to 90°, back to 0°, then to −90°, and lastly back to 0°. The change in electrical resistance (ΔR) is measured with a precision multimeter (Agilent 34401A). The scatter in data is attributed to the manual rotation of the clamps and can be mitigated with an automated testing platform.

4. Results

Experimentally measured values of ΔR are plotted versus κ for 6 mm thick PDMS (figure 5(a)) and EcoFlex®

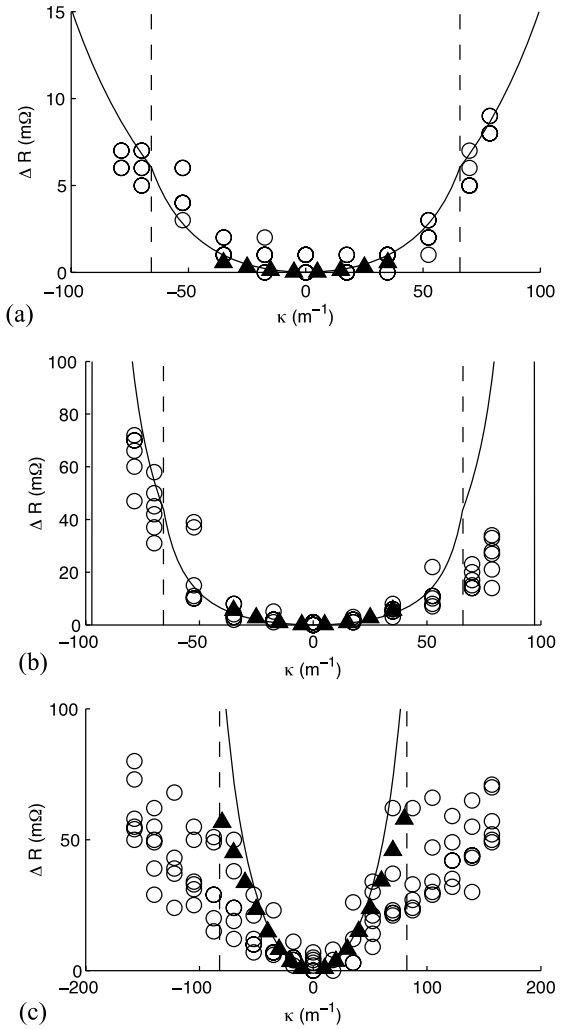

Figure 5. Change in electrical resistance ΔR as a function of pure bending curvature κ. Experimental measurements (open circles) and theoretical prediction (solid curve) for a 6 mm thick (a) PDMS and (b) Ecoflex® sensors and (c) a 1.3 mm thick PDMS sensor. The vertical dashed lines correspond to $\kappa = \kappa_{cr}$. For the 6 mm sensors, $L = 20$ mm, $g = 2$ mm, $\lambda = 26$ mm, $H = 0.5$ mm, $h = 2$ mm, $s = 2$ mm, $t = 0.4$ mm, $w = 3$ mm (PDMS), and $w = 1$ mm (Ecoflex®). For the 1.3 mm sensor, $L = 10$ mm, $g = 0.3$ mm, $\lambda = 16$ mm, $H = 50$ μm, $h = 0.5$ mm, $s = 1$ mm, $t = 0.1$ mm, $w = 0.8$ mm. The closed triangle markers correspond to theoretical predictions based on FEM solutions for f.

(figure 5(b)) sensors and a micropatterned 1.3 mm thick PDMS sensor (figure 5(c)). The sensors demonstrate the expected monotonic dependency of electrical resistance on absolute bending curvature. Nonetheless, there appears to be considerable scatter in the experimental data. This is predominately caused by the motion of the wires that connect the liquid microchannels with the multimeter. Because eGaIn has low electric resistivity, the external wiring and electrical connections contribute significantly to both the total resistance and resistance fluctuations. This may also explain why the more rigid 6 mm PDMS sample exhibits less scatter, since the embedded wires have less relative mobility. Other sources of scatter may include manual reorientation of the clamps and fluidic or viscoelastic effects in the sensor itself.

Theoretical predictions are also plotted in figure 5 and appear to be in reasonable agreement with the experimental measurements. Solutions based on a finite element (FEM) solution for f (COMSOL Multiphysics 4.0a, COMSOL AB) are plotted with closed triangle markers. These FEM solutions account for subcritical buckling induced by combined axial and moment loading in the plates and hence provide a more accurate estimate of the bending resistance. For the 6 mm thick PDMS sensor, the embedded channel is wider than the strut and so the collapse mode solution in equation (10) is used to predict ΔR. For the other two samples, the strut is wider and so the pressure mode solution in equation (2) is used. The theoretical curves for $|\kappa| > \kappa_{cr}$ are obtained by replacing the axial load f with f_{cr}, as described in section 2.3. These curves do not account for large plate buckling that would cause the gap to collapse. Nonetheless, we expect that when curvature is large ($\kappa > \kappa_{cr}$) collapse is possible and this will significantly reduce the sensitivity of the sensor.

For the results in figures 5(a) and (b), we observe reasonable agreement between theory and experiment. This indicates that the theoretical models are predictive, i.e. the ΔR–κ curve can be established a priori from prescribed sensor geometries (w, L, h, H, g, s, t, λ) and conductor resistivity (ρ). For figure 5(c), however, we find that the theory overestimates the sensitivity of the 1.3 mm PDMS sensor. One possibility is a slight misalignment between the strut and embedded channel, which will reduce the pressure exerted on the channel. While misalignments can also arise in the 6 mm sensors, the feature sizes are larger and so there will be less relative impact on performance. This may explain why the 6 mm sensors exhibit greater agreement with the theoretical and computational predictions.

Another possible source of discrepancy in figure 5(c) is the non-uniform transfer of internal stress from the strut to the plate. The theoretical predictions are based on the assumption that stress is uniformly distributed, i.e. $p = P/s\lambda$. While this approximation is reasonable for a thick film ($h \geqslant s$), it is no longer accurate when the film is thinner than the strut. This is apparent in figure 6, which shows the distribution of pressure obtained from a plane strain FEM analysis (COMSOL). In this simulation, $E = 167$ kPa, $\nu = 0.45$, $s = 2$ mm, $g = 2$ mm, the thickness of the outer plate is $h = 1$ mm, and the thickness of the inner plate is $h = 7$ mm. For the thicker plate, compressive stress appears to be uniformly distributed throughout the junction between the plate and strutt. However, for the thinner plate, the internal pressure is concentrated away from the center point where the channel would be embedded. In this case, $p = P/s\lambda$ would lead to an overestimate of ΔR.

5. Discussion

Bending curvature κ is determined by measuring the change in electric resistance ΔR of an embedded microchannel of conductive liquid. A closed-form algebraic estimate for the relationship between ΔR and κ is derived from elastic plate theory. The theoretical predictions are in reasonable agreement with experimental measurements obtained for a variety of sensor geometries and materials. In contrast to existing

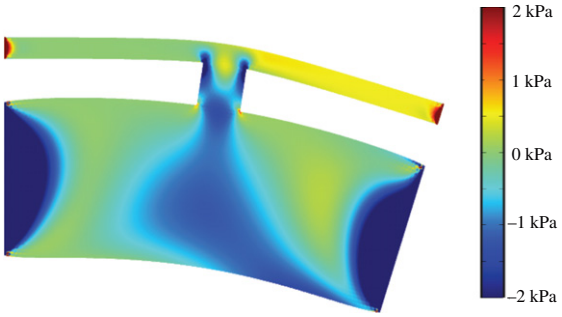

Figure 6. Internal pressure obtained from a plane strain FEM analysis (COMSOL). The stress on the outer (thinner) plate is concentrated at the corners of the junction and away from the center of the strut. For the inner (thicker) plate, pressure is distributed uniformly throughout the connection between the plate and strut.

curvature sensors, the sensor presented here is composed entirely of soft and stretchable materials and can measure curvature directly on the neutral bending plane.

Curvature sensing represents just one capability necessary to completely map the shape and deformation of an elastic body. Complete shape mapping can be accomplished by combining curvature sensors with strain (Kim *et al* 2008) and pressure sensing (Park *et al* 2010). Since all of the sensing elements scale differently with stretch, curvature, and pressure, it is possible to decouple these values by comparing each sensor measurement ΔR. This may be done mathematically from the algebraic expressions for ΔR or graphically from the sensor response curves.

5.1. Bi-directional sensing

In order to determine the sign of bending curvature, two curvature sensors must be placed on top of each other. Due to the buckling-induced asymmetry, the sensor embedded inside the inner film will register a smaller change in electrical resistance. Therefore, the sign of bending curvature is determined by identifying the sensor with the smaller measured ΔR. Alternatively, two curvature sensors may be placed side-by-side with thicker backings on opposite surfaces to induce buckling asymmetry. In both cases, the film containing the sensor must be sufficiently thin so that buckling occurs below the prescribed sensitivity threshold.

5.2. Gauge factor

Conventional curvature sensors use differential strain, in which a strain sensor is placed off of the neutral axis by a distance z and measures a strain $\varepsilon = \kappa z$. For these sensors, the gauge factor GF is defined as the ratio of the relative change in electrical resistance to the corresponding strain, i.e. GF $= (\Delta R/R_0)/\varepsilon$. For elastomer-based strain sensors (Kim *et al* 2008), $\Delta R/R_0$ is approximately 2ε and so GF ~ 2 and is invariant to film thickness or material.

In contrast, the curvature sensors presented here do not have a fixed GF and $\Delta R/R_0$ is scale invariant to total thickness $Z = 2h + g$. Dividing by $\varepsilon = \kappa z$ yields the equivalent gauge factor:

$$\mathrm{GF} = \frac{1}{(2h+g)\kappa}\left\{\frac{1}{1-\chi\kappa h\sin(\kappa L/2)} - 1\right\} \qquad (14)$$

where χ equals $\alpha = 2w(g+h)/Hs$ or $\beta = (g+h)(3s+w)(w-s)^3/64wHt^3$ depending on the mode of channel deformation. Therefore, any arbitrary gauge factor can be achieved for a prescribed bending curvature κ by selecting the appropriate sensor geometries.

6. Conclusion

In closing, a hyperelastic, soft microfluidic film measures bending curvature using a novel non-differential mechanism. In contrast to conventional curvature sensors that use a strain sensor offset from the neutral axis, this elastomer-based solution allows for curvature sensing directly on the bending plane and thus eliminates limitations imposed by strain gauge factor (GF) and sensor thickness (Z). Future efforts will focus on the integration of non-differential curvature sensing into a stretchable, softer-than-skin elastomer that completely maps shape and surface pressure.

Acknowledgments

This work was funded by the National Science Foundation, award number DMR-0820484 (CM) and the Wyss Institute for Biologically Inspired Engineering (RK). Any opinions, findings and conclusions or recommendations expressed in this material are those of the authors and do not necessarily reflect those of the National Science Foundation.

References

Cheng S and Wu Z 2010 Microfluidic stretchable RF electronics *Lab Chip* **10** 3227–34

Cheng S and Wu Z 2011 A microfluidic, reversibly stretchable, large-area wireless strain sensor *Adv. Funct. Mater.* **21** 2282–90

Dickey M D, Chiechi R C, Larsen R J, Weiss E A, Weitz D A and Whitesides G M 2008 Eutectic gallium–indium (EGaIn): a liquid metal alloy for the formation of stable structures in microchannels at room temperature *Adv. Funct. Mater.* **18** 1097–104

Gere J M and Timoshenko S P 1984 *Mechanics of Materials* 2nd edn (Boston: PWS-Kent) pp 551–69

Hawkes E, An B, Benbernou N, Tanaka H, Kim S, Demaine E D, Rus D and Wood R J 2010 Programmable matter by folding *Proc. Natl Acad. Sci. USA* **107** 12441–5

Khang D-Y, Jiang H, Huang Y and Rogers J A 2006 A stretchable form of single-crystal silicon for high-performance electronics on rubber substrates *Science* **311** 208–12

Kim D-H, Ahn J-H, Choi W M, Kim H-S, Kim T-H, Song J, Huang Y Y, Liu Z, Lu C and Rogers J A 2008 Stretchable and foldable silicon integrated circuits *Science* **320** 507–11

Kim H-J, Son C and Ziaie B 2008 A multiaxial stretchable interconnect using liquid-alloy-filled elastomeric microchannels *Appl. Phys. Lett.* **92** 011904

Kramer R, Majidi C and Wood R J 2011 Wearable Tactile Keypad with Stretchable Artificial Skin *ICRA: Proc. Int. Conf. Robotics & Automation (Shanghai)*

Park Y-L, Chen B-R, Paul C, Young D, Stirling L, Wood R J, Goldfield E and Nagpal R 2011 Bio-inspired active, soft

orthotic device for treating gait pathologies *IROS: Proc. Int. Conf. Intelligent Robots & Systems (San Francisco, CA)*

Park Y-L, Majidi C, Kramer R, Berard P and Wood R J 2010 Hyperelastic pressure sensing with a liquid-embedded elastomer *J. Micromech. Microeng.* **20** 125029

Quake S R and Scherer A 2000 From micro- to nanofabrication with soft materials *Science* **290** 1536–40

Rogers J A and Huang Y 2009 A curvy, stretchy future for electronics *Proc. Natl Acad. Sci. USA* **106** 10875–6

Seok S, Onal C D, Wood R J, Rus D and Kim S 2010 Peristaltic locomotion with antagonistic actuators in soft robotics *ICRA: Proc. Int. Conf. Robotics & Automation (Anchorage, AK)*

So J-H, Thelen J, Qusba A, Hayes G J, Lazzi G and Dickey M D 2009 Reversibly deformable and mechanically tunable fluidic antennas *Adv. Funct. Mater.* **19** 3632–7

Xia Y, Rogers J A, Paul K E and Whitesides G M 1999 Unconventional methods for fabricating and patterning nanostructures *Chem. Rev.* **99** 1823–48